Time-Resolved Photoluminescence Spectra of Si Species Encapsulated in Zeolite Supercages

Katsumi Tanaka,*,† Yuhko Komatsu,‡,§ and Cheow-Keong Choo†

Department of Human Communication and Graduate School of Electronic Engineering, The University of Electro-Communications, 1-5-1 Chofu, Tokyo 182-8585, Japan

Received: June 18, 2004; In Final Form: October 21, 2004

Photoluminescence (PL) spectra of Si species encapsulated in zeolite supercages are studied. It is reported that the chained Si species terminated partially with phenyl groups and with some unsaturated bonds are formed in zeolite supercages by the reaction with phenylsilane and they show PL around 4 eV (*J. Phys. Chem.* **2004**, *108*, 2501−2508). In the present paper they are reduced with hydrogen to prepare Si chained species terminated and saturated with hydrogen atoms. The PL spectra are deconvoluted to be four components at 1.9, 2.2, 2.6, and 3.7 eV, which can tentatively be assigned to Si nanocrystals and Si quantum wires in addition to defects in SiO_2 and uncontrolled organic impurities in zeolite, respectively. At elevated temperatures the Si quantum wires in zeolite pores seem to change the Si nanocrystals with the size larger than that of the zeolite pore diameter. It is the first case in which the PL decay lifetime of oxygen vacancies in zeolite can be detected to be quite short to be about 16 ns. The detected lifetimes of Si quantum wires are significantly very short, about 12 ns. The Si species encapsulated zeolite is solvated with hydrofluoric acid solution to separate the Si quantum wires by dissolving zeolite lattice. The Si quantum wires in the HF solution show intense PL spectra peaked at 2.33 eV and broad UV spectra around 2.8−3.5 eV. They will have different shapes and lengths. The HF solvated zeolite shows still PL spectra characteristic of oxygen vacancies and the absorption edge at 3.6 eV. The result means that zeolite lattice is solvated in HF solution as clusters with a band gap of 3.6 eV and they can still have some oxygen vacancies. Oxygen vacancies situate about 1.0 eV below the zeolite conduction band minimum, and the absorbed energy can be dissipated as PL between the valence band maximum and the oxygen vacancies. It is concluded that the excitation photon energy can be absorbed in zeolite and the Si quantum wires and then the absorbed energies are competitively relaxed in zeolite and the Si quantum wires.

Introduction

Zeolites are inorganic aluminosilicate materials composed of three-dimensional pore structures with different sizes and there are many types of zeolites with different pore structures.[1] One of the most significant interests in zeolites seems to lie in the use of pores as a vessel for occlusion chemistry and for synthesis of dimension-defined materials.[2] So far, many challenges have been trying to make sub-nanometer-sized clusters,[3−7] semiconductors,[8−13] and polymers[14−16] in zeolite pores. On the other hand, the one-dimensional channels of $AlPO_4$-5 molecular sieves have also been used as a vessel for the synthesis of dimension-defined materials such as carbon nanotube synthesis[17] as well as molecular alignments for the optical second harmonic generation.[18] The inner surface of a molecular sieve $AlPO_4$-5 is very inert, and it is difficult to make strong chemical bonds with functional groups since no hydroxyl group exists. In this sense, not only the zeolite but also the molecular sieve inclusion chemistry gathers much interest.[19] We have tried to include Si clusters in the $AlPO_4$-5 pores by thermal diffusion.[20−22] We have detected the band gap of the N-terminated Si clusters at 2.2 eV [22] and observed the emission from Si clusters at 2.25−2.07 eV, depending on the size.[23] Although encapsulated II−VI group semiconductor clusters in zeolites have been widely studied,[24,25] only a few works have been carried out on silicon clusters encapsulated in zeolite pores. Recently silicon nanoclusters with an average value of 12 ± 2 Si/cluster have been successfully encapsulated in zeolite−Y cavities through bonding with zeolite framework OH groups.[26,27] The encapsulated silicon species are clusterized by thermal treatment at 773 K, and as a result the clusters are air-stable and exhibit a room-temperature photoluminescence (PL) in the green-yellow region at 2.2 eV.

Since the discovery of visible-region PL in porous Si,[28] it has been expected that downsizing the bulk silicon to nanoscale induces a more efficient PL even at 298 K with direct transitions as well as the emission wavelength shift to the visible region.[29] The PL intensity of bulk Si in the near-infrared drastically drops as the temperature increases, whereas that of nanowires does not so decrease between 0 and 100 K.[30] It has been found that the PL lifetimes τ_{PL} of nanosilicon species become shorter as the temperature increases;[31] however, they are relatively slow and are found to be in millisecond regions even at 298 K. The τ_{PL} of nanosilicon species at 2.14 eV is very short, 20 ns at near 0 K, but decreases to 3 ns at 150 K.[32] The PL lifetime becomes short in the case of the exciton recombination as the size of the particles becomes small since a nonphonon process is dominant.[33,34] On the other hand, the lifetime of PL at 1.4 eV becomes longer (1.5 ms at 5 K to 160 ms at 298 K) in nanocrystalline Si prepared in inert gas due to phonon dispersion.[35] In addition, the PL component with very short τ_{PL} below 40 ns is also observed in the system. Furthermore, the PL lifetime of Si species at 2.1 eV can be estimated to be 0.1−1

* Corresponding author. E-mail: tanaka@hc.uec.ac.jp.
† Department of Human Communication.
‡ Graduate School of Electronic Engineering.
§ Present address: SEIKO-EPSON Corp.

10.1021/jp047355f CCC: $30.25
Published on Web 12/07/2004

μs.[36] As a result, the origin and the lifetime of PL spectra in nanosilicon species are still mysterious.

The authors recently reported that chained Si species with about 30 Si atoms are synthesized in zeolite pores by the reaction with phenylsilane ($PhSiH_3$) at 423 K.[37] It is assumed that they will be polysilane families terminated with some phenyl groups and they will also have some unsaturated bonds between Si and Si. They show intense PL spectra around 4 eV and can be extracted in hexane at 298 K. The extracted species also show red-shifted intense PL spectra peaked at 4.07 eV and the broad UV spectra due to the polysilane backbone structure at 220−280 nm. It is concluded that polysilane families absorb excitation photon energy and relax to show PL characteristic of the Si backbone structure.[37] In the present paper, such polysilane families in zeolite pores are reduced with hydrogen at 573, 673, and 1073 K to saturate the unsaturated bonds with hydrogen atoms and simultaneously to substitute phenyl groups into terminated hydrogen atoms. In addition, the photoluminescence behaviors of formed Si species are studied with nanosecond time-resolved analysis. The decay lifetimes of Si species in zeolite pores are nearly at the nanosecond detection limit in our system and are significantly very short (about 12 ns) compared to the nanosized Si so far reported. The formed Si species are separated from zeolite by dissolution of zeolite lattice in hydrofluoric acid solution, and the solvated Si species are studied with ultraviolet spectra and photoluminescence spectra.

Experimental Section

The preparation methods of polysilicon species in zeolite supercages with phenylsilane ($PhSiH_3$) are described in our previous paper.[37] The faujasite zeolite used was the HY zeolite (Tosoh Corp.) with a SiO_2/Al_2O_3 ratio of 5.6 and surface area of 570 $m^2\ g^{-1}$, in which 68% of Na ions of the starting Na−Y (surface area of 700 $m^2\ g^{-1}$) had been changed into H ions. The X-ray diffraction (XRD) pattern of the HY zeolite powder showed a crystal structure similar to the Na−Y zeolite. The powder of 0.5 g was pressed at 150 $kg\cdot cm^{-2}$ between two metal barrels and was changed to the pellet for photoluminescence. The pellet was treated with 1 atm of flowing oxygen gas in a quartz tube at 673 K for several hours to remove the organic residues. It is found that the (111) face of zeolite become intense after the oxygen treatment because the crystallinity is increased as oxygen vacancies are removed.[37] The pellet was transferred to an ultrahigh-vacuum stainless chamber system evacuated with a 150 L/s turbo molecular pump back-supported with a 100 L/min rotary pump. The base pressure of the system was below 1×10^{-6} Pa. The pellet was evacuated at 673 K by resistive heating with tungsten wire for 1 h. The temperature was measured with a thermocouple. The zeolite pellet was reacted with 6.65 hPa (5.0 Torr) of phenylsilane at 423 K in the closed system for 2 h. The reaction with phenylsilane at 423 K was repeated several times. The sample was evacuated at the same temperature in the intervals of the reactions with phenylsilane. The phenylsilane liquid ($PhSiH_3$: Shin-Etsu Chemicals, purity >99.5%) was reserved in glass vessels and was degassed at several freeze−pump−thaw cycles. The polysilane species are formed in the zeolite supercages, and characterization with FT-IR, Q-mass, UV, PL, and X-ray photoelectron spectroscopy (XPS) is reported in the previous paper.[37] Hereafter the zeolite in which polysilane species have been formed in the supercages is denoted as the polysilane/zeolite.

The polysilane/zeolite pellet was exposed to air at 298 K and then transferred to the quartz tube. Hydrogen gas was flowed (about 60 mL/min) in the quartz tube at 298 K for 10 min during which air was changed to hydrogen completely. The treatment with hydrogen was carried out in the quartz tube at 573, 673, and 1073 K for 1 h, respectively. Hereafter the hydrogen-reduced polysilane/zeolite samples are denoted as Si/zeolite; for instance, the sample reduced at 573 K is denoted as Si/zeolite-573K. After the treatment with hydrogen, the temperature of the system was dropped to 298 K. Then the hydrogen flow was changed to a nitrogen flow, and the flow was continued for 20 min. For the PL experiments, the Si/zeolite sample was transferred to the ultrahigh-vacuum chamber and evacuated at 573 K for 30 min.

Photoluminescence spectra were analyzed with a multichannel photodetector (Hamamatsu photonics PMA-11, C7473-36) at 298 K. The wavelength-dependent intensity response was automatically corrected in this system. PL spectra were excited by pulsed laser shots at 266 nm (Continuum, Surelite 10, at 4 ns and 10 Hz) and were recorded in vacuo. The laser light was introduced to the surfaces with 45° off-normal, and the luminescence was measured with surface normal. The glass window was put to the metal-made probe guide end to avoid reflection of laser light at 266 nm. However, the excitation light at 266 nm could not be removed completely. The PL spectra in the wavelength scale are converted to that in the energy scale to deconvolute the PL components. Precisely speaking, an intensity in wavelength scale $\Phi(\lambda)$ and the corresponding intensity in energy scale $\Phi(E)$ reach the relation $\Phi(\lambda)\,d\lambda = \Phi(E)\,dE$ since photon energy for the relaxation is constant. Since $dE = -(hc/\lambda^2)\,d\lambda$ is derived from $E = hc/\lambda$, $\Phi(E)$ corresponds to $\Phi(\lambda)\lambda^2\alpha$. Here α is a constant. As the direction dE and $d\lambda$ is opposite, the negative sign is canceled. Such a correction was carried out in the present study. It was found that the energy-scale emission peaks were shifted to the lower energy side only about 0.05−0.08 eV at maximum considering the λ^2 correction factor in visible PL spectra.[38,39]

The time-resolved PL system we used was in detail described in the previous papers.[38] The pulsed 355 nm laser oscillated in a Nd:YAG laser (Continuum, Powerlite 9010) used to excite the zeolite and the Si/zeolite samples. PL spectra were collected with a cylindrical lens and were analyzed with the optical multichannel analyzer (OMA), which was composed of a monochromator (Oriel Instruments; MS257) and an intensified charge-coupled device (ICCD; Andor) detector. A time sequence for one time-resolved PL analysis of the flash lamp, Q-switch, and delay as well as width for one data collection was controlled with a digital delay/pulse generator (DDG; Tokyo Instruments DG535). The time diagram was as follows. The width was constant at 300 ns, and the delay time was controlled so as to be a time zero when an intensity of excitation laser light was maximized for the time-resolved PL decay spectrum. The data were collected at 10 Hz to be integrated. The Si/zeolite-673K was supplied to time-resolved PL analysis. The reason is that the PL component at 2.2 eV is most intense in the sample.

Based on the same reason, the Si/zeolite-673K was dissolved in hydrofluoric acid (HF). The zeolite itself was also dissolved in hydrofluoric acid for comparison. These solutions were transferred to PMMA UV cells and were studied with an UV/vis spectrophotometer (JASCO Ubest-30). The solutions in PMMA cell were supplied to PL measurements.

Results

X-ray diffraction spectra of zeolite (a−c) and the Si/zeolite (d−f) are shown in Figure 1. When the fresh H−Y zeolite was oxidized with oxygen at 673 K, the intensity of the (111) peak around 6° was increased as shown from b to a. The result has

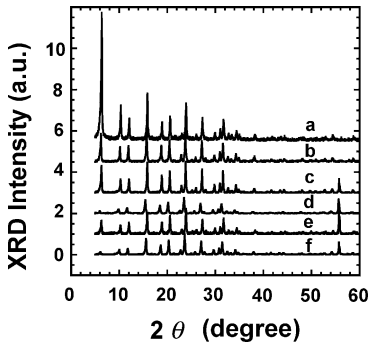

Figure 1. X-ray diffraction patterns of the HY-68 zeolite oxidized at 673 K (a), as obtained (b), HY reduced with H_2 at 1073 K (c), Si/zeolite-573K (d), Si/zeolite-673K (e), and Si/zeolite-1073K (f).

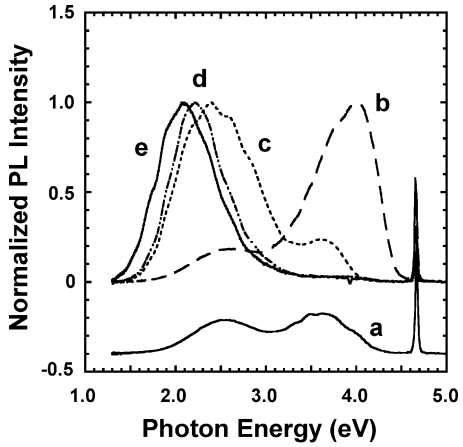

Figure 2. PL spectra of the HY zeolite as obtained (a), polysilane/zeolite (b), Si/zeolite-573K (c), Si/zeolite-673K (d), and Si/zeolite-1073K (e). They are excited at 266 nm (4.66 eV) at 298 K as revealed by the sharp spike in the figure. The PL intensities of b−e are normalized, and PL spectrum a is shown for comparison with no normalization.

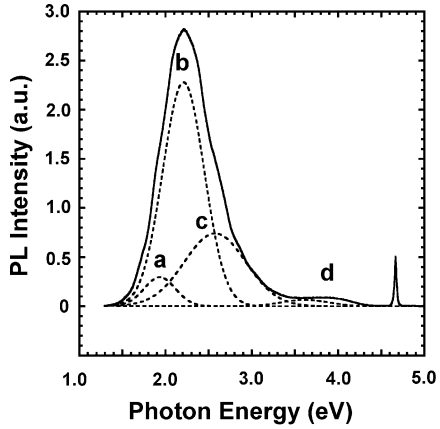

Figure 3. Deconvolution of the PL spectrum on Si/zeolite-673K. The PL spectrum is the same as Figure 2d but with real intensity. The PL intensity can be compared with Figure 4.

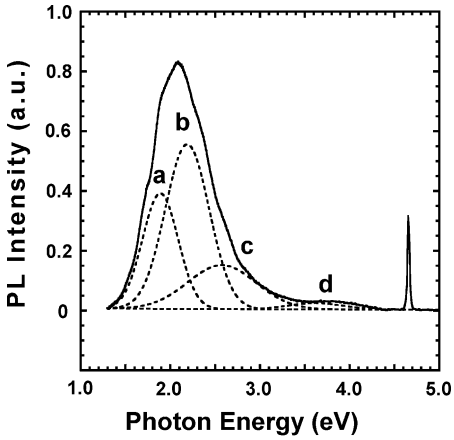

Figure 4. Deconvolution of the PL spectrum on Si/zeolite-1073K. The PL spectrum is the same as Figure 2e but with real intensity. The PL intensity can be compared with Figure 3.

been already reported and is explained by the enhancement of crystallinity as being oxygen vacancies removed.[37] The structure of the zeolite was reserved after reducing it with hydrogen at 1073 K (c). The peak at 56° is assigned to the Ta holder which is used to hold zeolite pellets. The oxidized zeolite was reacted with $PhSiH_3$ at 423 K several times to prepare the polysilane/zeolite samples. The XRD spectrum of the Si/zeolite-573K shows that the (111) peak is drastically diminished and the intensities of the other peaks also decrease. The result implies that the crystal structure of the supercages is distorted probably because they are occupied by the products formed by the thermal reaction of polysilane with hydrogen. When the hydrogen treatment temperature was increased to 673 K, then the XRD peak intensities increased again, shown in e. The XRD peak intensities decreased to the same order as at 573 K after reducing the sample at 1073 K (f). It is found that the crystal structure of zeolite is extremely stable even by reducing with hydrogen at 1073 K; however, the structure is distorted by the products in the supercages by the reaction of polysilane with hydrogen.

Figure 2 shows the PL spectra of zeolite as obtained (a), the polysilane/zeolite (b), and the Si/zeolite-573K (c), -673K (d), and -1073K (e), respectively. The PL intensities of b−e are normalized, and the PL of zeolite is shown for comparison in an arbitrary intensity. It is reported in the previous paper that the formed polysilanes are composed of about 30 Si atoms with some unsaturated bonds between Si and Si and are also terminated with some phenyl groups.[37] In addition, the PL peaks at 2.7, 3.6, and 4.0 eV could be assigned to oxygen vacancies in zeolite, uncontrolled organic impurities, and the polysilanes in supercages, respectively. The PL spectrum of Si/zeolite-573K (c) showed a peak around 2.4 eV with small peak at 3.6 eV. The PL peak shifted to lower photon energy to 2.2 and 2.1 eV in Si/zeolite-673K and Si/zeolite-1073K, respectively. The two PL spectra are deconvoluted as shown in Figures 3 and 4, in which PL intensities can be compared. In Figure 3, the PL spectrum can be deconvoluted into four species at 1.9, 2.2, 2.6, and 3.6−4.0 eV. It is very clear that the PL component at 2.6 eV assigned to oxygen defects in zeolite is present for the PL spectra in Figures 3 and 4. It is noted that the PL intensity at 1.9 eV of the Si/zeolite-673K is almost the same as that of the Si/zeolite-1073K. In addition, it is assumed that the PL component at 2.2 eV seems to decrease after reduction with hydrogen at 1073 K. It is significant to point out that the PL intensity at 2.6 eV diminishes in the Si/zeolite-1073K. One can imagine that oxygen vacancies will be increased by the reduction with hydrogen at higher temperature. In Figure 1f, the XRD intensity of zeolite (111) of $2\theta = 5°$ is completely suppressed in Si/zeolite-1073K, although the other diffraction peaks show some intensities. The result implies that zeolite supercages will be crashed or fulfilled with the formed Si species. Oxygen vacancies will be destroyed simultaneously, for instance by the reaction with the Si species. The deconvolution at higher photon energy region does not seem to fit so well because only one component is estimated at 3.6 eV. If the PL component at 4.0 eV is added for the deconvolution, the best fit could be obtained. At this moment, it is not certain whether the polysilane families

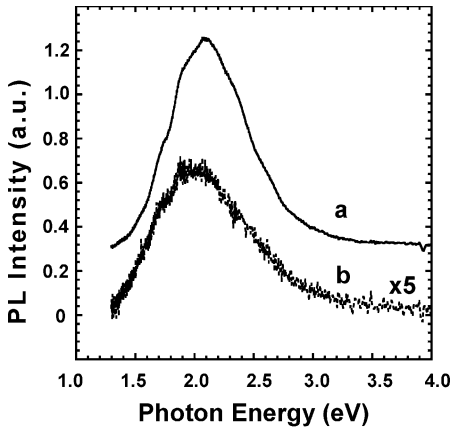

Figure 5. PL spectra of the tail surface (a) and the head surface (b) of the Si/zeolite-1073K pellet. Spectrum a is the same as in Figure 2e. The PL intensity can be compared with Figure 4.

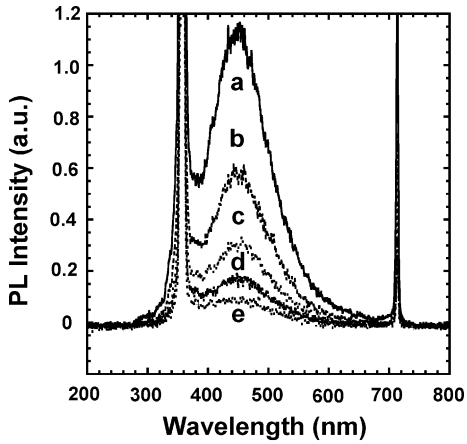

Figure 6. Time-resolved PL spectra in the HY reduced with H_2 at 673 K measured at 298 K. The PL spectra shown are delayed at 0 (a), 10 (b), 20 (c), 30 (d), and 40 ns (e).

formed by the reaction with phenylsilane at 423 K can survive as the native form after reacting with hydrogen at 1073 K, probably not.

The Si/zeolite-1073K pellet showed two kinds of PL spectra as shown in Figure 5. The head surface showed a light charcoal color, whereas the color of the tail surface was white. When the sample was reduced with hydrogen at 1073 K, the tail surface touched the quartz furnace directly and hydrogen gas was flowed on the head surface. The temperature of the head surface will probably be lower than that of the tail surface because of hydrogen flow. The deposition of the Si species will be responsible for the charcoal color on the head surface. Such deposited Si showed weak PL spectra peaked at around 2.0 eV with some shoulders at 1.7 and 1.9 eV. The PL spectrum is unsymmetrical, and the broad skirt can be detected in the higher photon energy side. It is noted that the PL component at 1.7 eV is dominantly detected on the deposited Si species. As the diameter of the entrance of zeolite pores is 0.7 nm, the Si species formed in zeolite supercages with a size smaller than 0.7 nm can be extracted from supercages to the external surface and will be deposited probably as Si nanocrystals.

In Figures 6 and 7, the time-resolved PL spectra in the zeolite reduced with hydrogen at 673 K and Si/zeolite-673K are shown, respectively. The sharp spikes at 355 and 710 nm are the excitation laser to the time-resolved system and the overtone, respectively. It is noted that the PL spectra in Figures 2−4 are excited at 266 nm. The PL spectra delayed at 0, 10, 20, 30, and 40 ns are shown in a−e in two figures. The PL around 460 nm

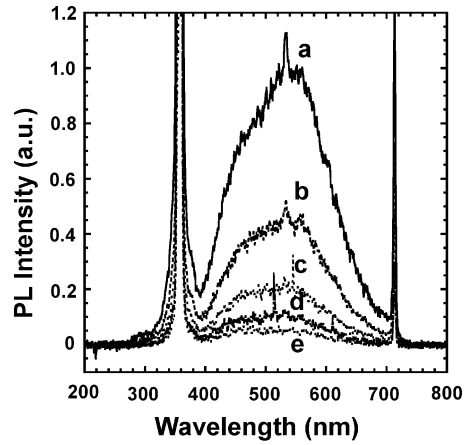

Figure 7. Time-resolved PL spectra in Si/zeolite-673K measured at 298 K. The PL spectra shown are delayed at 0 (a), 10 (b), 20 (c), 30 (d), and 40 ns (e).

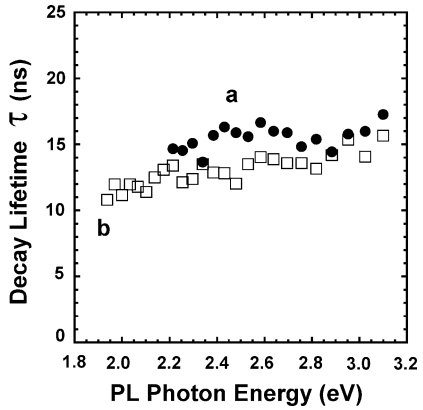

Figure 8. PL decay time as a function of the PL photon energy of HY zeolite reduced with H_2 at 673 K (a) and Si/zeolite-673K (b).

in zeolite originates from oxygen vacancies in zeolite selectively. The PL around 500−700 nm is quite significant in Figure 7 and can be assigned to Si species in zeolite. Best fit analysis of total PL intensity $I(t)$ as a function of time t can be obtained by assuming the linear combination of PL decay components as follows.

$$I(t) = I \exp(-t/t_{PL}) + I' \exp(-t/\tau_{PL'}) + I'' \exp(-t/\tau_{PL''}) + ... \quad (1)$$

Here I and τ_{PL} for the first term represent the PL intensity of the decay component at time zero and the luminescence lifetime, respectively. The same is represented for the other PL components in the second and the third terms, and so on. It was found that only one PL decay component could yield a best fit for the total PL intensity decay curve as a function of time in Figures 6 and 7. The decay lifetime, τ_{PL}, in zeolite and that in Si/zeolite-673K are shown in Figure 8 as a function of PL photon energy. The lifetime of oxygen vacancies in zeolite around 2.6 eV is quite short, about 16 ns. To our knowledge, it is the first case in which the PL decay lifetime of zeolite can be obtained. The decay lifetime seems independent of the PL wavelength. Compared to PL in zeolite, the PL lifetimes of Si species in zeolite can be studied at 1.9−2.2 eV, although some contribution from oxygen vacancies is involved. The values are about 12 ns and seem shorter than those of PL in zeolite. It is significant that our detection limit is about 10 ns and our pulse laser width is 4 ns so that the value of 12 or 16 ns for PL decay lifetimes may be estimated to be much shorter and should be the slowest

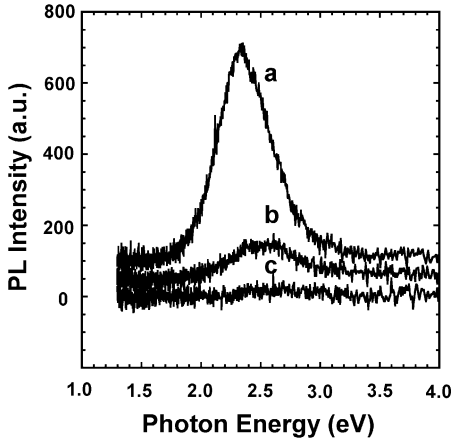

Figure 9. PL spectra of the HF solvated solutions of Si/zeolite-673K (a) and HY reduced with H_2 at 673 K (b). The solutions are measured in PMMA cell. For comparison the HF solution in PMMA cell is shown in c.

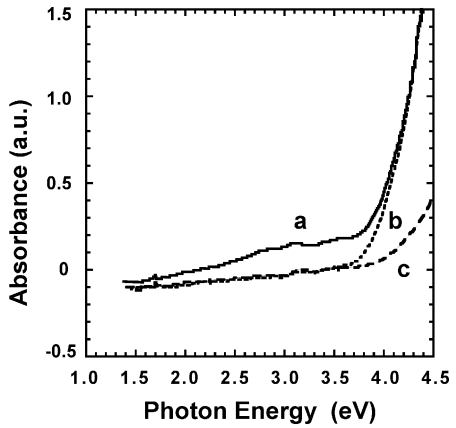

Figure 10. UV/vis absorption spectra of the HF-solvated solutions of Si/zeolite-673K (a) and HY reduced with H_2 at 673 K (b) as a function of the excitation photon energy. Note that spectrum c corresponds to the absorption spectrum of PMMA since the same spectrum can be obtained with and without HF solution.

ones. In this sense, the PL components with much shorter decay lifetimes may exist; however, they cannot be detected in our system.

To eliminate the contribution from oxygen vacancies on the PL analysis of Si species in zeolite supercages, Si/zeolite-673K was dissolved in HF solution. The solvated solution showed charcoal color. On the other hand, it became a transparent solution after zeolite itself was solvated with HF. Therefore, it is found that the solvated Si species are responsible for the charcoal color. Two solutions were reserved in PMMA cells and were supplied to PL measurements and UV analysis. As shown in Figure 9c, HF solution in PMMA shows no PL spectra. However, the zeolite-solvated HF solution shows weak PL peaks at 2.4 and 2.6 eV in b. The PL peaks will be associated with oxygen vacancies in zeolite assigned in Figures 3 and 4. If it is the case, the solvated zeolite should have still some cluster sizes with oxygen vacancies. Spectrum a in Figure 9 shows an intense PL peak centered at 2.35 eV, which is originated from PL components analyzed at 1.9 and 2.2 eV in Figures 3 and 4. The two HF solutions were analyzed with UV/vis spectra. Figure 10 shows these spectra as a function of photon energy in electronvolts. As a reference, the HF solution in PMMA cell as well as PMMA cell absorbs the photon energy below 3.8 eV, as shown in Figure 10a. The result implies that UV spectrum c in Figure 10 is attributed from PMMA. In addition, the zeolite

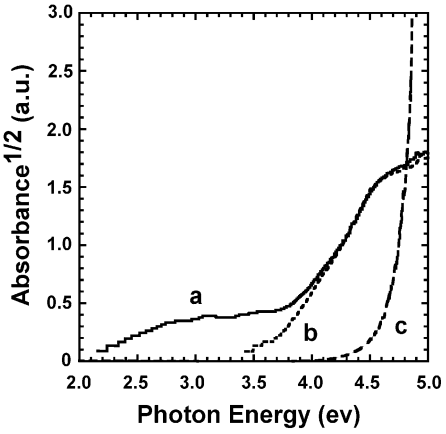

Figure 11. Plot of the square root of absorbance as a function the excitation photon energy for the indirect transitions. The data of a−c in Figure 10 are used, and the notations are the same.

solvated in HF solution also absorbs the photon energy below about 3.7 eV. Compared to these two spectra, the HF-solvated Si species showed about three absorption maxima at 2.8, 3.1, and 3.5 eV in Figure 10a.

For the indirect transitions between indirect valleys (eq 2) and for allowed direct transitions (eq 3) of materials with band gap E_g, the absorbance values α are proportional to the square root and the square of photon energy, respectively.[40] Here, C and D are constants.

$$\alpha(h\nu) = C(h\nu - E_g)^2 \tag{2}$$

$$\alpha((h\nu)) = D(h\nu - E_g)^{1/2} \tag{3}$$

In Figure 11, the square-root of absorbance is plotted as a function of photon energy to study the band gaps in the indirect transitions of solvated zeolite and the solvated Si species supplied from the reaction of polysilane in zeolite supercages with hydrogen at 673 K. The absorption edge of the PMMA cell can be extrapolated to 4.7 eV. It is quite significant to note that the band gap of dissolved zeolite in HF is extrapolated to 3.6 eV. As mentioned in Figure 9, the PL in dissolved zeolite in HF can reflect the nature of oxygen vacancies as it should have in the bulk structure. If the nature of the bulk structure of zeolite is also reflected in the UV/vis spectrum in the HF solution, one can conclude that the band gap of zeolite will be 3.6 eV in the indirect transitions. The band gap of Si nanocrystals solvated in HF can be extrapolated to 2.0 eV.

Discussion

(a) Assignment of PL Species. In the present study, the polysilane/zeolite sample was reduced with hydrogen to change the polysilane families to Si species with PL in visible region. The aim of hydrogen treatment is to cause the substitution reaction of the terminated phenyl groups into hydrogen atoms and simultaneously to saturate the unsaturated bonds such as Si═Si with them. It is expected that the hydrogen treatment of the polysilane/zeolite sample will lead to a way of synthesis of Si nanowires or the ladder structures. The disadvantage of hydrogen reduction is that oxygen vacancies will be formed in a zeolite framework and they should show the characteristic PL. If the polysilane/zeolite is oxidized with oxygen, oxygen vacancies should decrease. However, Si−O related species and Si/SiO_2 interface also show PL at 3.35 eV even after oxidation.[41,42] We consider that polysilanes formed in zeolite supercages should be oxidized with oxygen. Then, it will be difficult

to distinguish these species from a zeolite framework composed of SiO_4 tetrahedra. As a result, we consider that hydrogen treatment is much more convenient for studying the PL components in zeolite supercages.

The PL at 2.7 eV has been detected in neutral oxygen vacancies defects in silica.[43,44] We also assigned PL species at 2.7 eV to oxygen vacancies in zeolite.[37] It is based on the fact that the PL at 2.7 eV diminishes after oxidizing zeolite at 673 K. The zeolite framework is composed of $[SiO_4]^{4-}$ tertahedra with some substituted $[AlO_4]^{5-}$. In this sense, the PL component observed at 2.6 eV in our experiments will be reasonably assigned to oxygen vacancies. Such a PL component can be observed after the zeolite itself is dissolved in HF solution, as shown in Figure 9. The result implies that some zeolite frameworks remain and they retain oxygen vacancy sites as in the bulk state. This holds true in Figure 11, in which it is significantly concluded that the band gap of zeolite is 3.6 eV. Then, the photon at 355 nm (3.49 eV) as excitation for the time-resolved PL detection system can be resonantly absorbed. PL measurements are carried out at 298 K so that zeolite lattice will be vibrated thermally enough to be able to absorb photon at 355 nm. Therefore PL spectra will be quite similar at excitation with 266 and 355 nm. It is concluded that oxygen vacancies situate about 1.0 eV below the conduction band minimum of zeolite and the energy difference between oxygen vacancies and the valence band maximum correspond to PL at 2.6 eV.

The polysilane synthesized in zeolite pores showed the PL at 4 eV. In general, polysilanes should be terminated with hydrogen atoms. However, the polysilanes formed by the reaction with phenylsilane in zeolite supercages contain phenyl groups and unsaturated bonds. In addition, the backbone structure and lengths will be inhomogeneous in zeolite.[37] Therefore, it may be reasonable to term them as polysilane families. The polysilane families are changed to the Si species after hydrogen treatment, which show characteristic PL peaks at 2.2 and 1.9 eV. Here the assignment of the species is discussed.

So far, it has been reported that the Si nanoparticles show the typical PL at 1.6 eV, which is assigned to the recombination of the excitons confined in them.[45−48] It is also reported that the PL peak energy depends on the diameter of the Si nanoparticles as follows.[48]

$$E_g = E_g^{bulk} + Ad^{-1.34} \quad (4)$$

Here E_g^{bulk} and d represent the band gap of bulk Si (1.1 eV) and the diameter of the Si nanoparticles, respectively. According to their assumption, the diameter with PL peaked at 1.9 eV corresponds to 3.2 nm. One is reminded that the inner diameter of supercages in HY zeolite is 1.3 nm. However, the size of Si nanoparticles should be smaller than the inner diameter of supercages in HY zeolite unless some of the polysilane families are converted to the species in the pores. It is also quite significant that the PL peak is constant at 1.9 eV, although the PL intensity changes as the hydrogen treatment temperature increases. This fact implies that the PL peak does not shift with the size of the Si species or the Si species are no more encapsulated in zeolite supercages but situate outside the pores. One of the new man-made Si materials has been prepared recently and shows typical red-shifted PL as the size increases.[49] The PL peak shifts from 1.7 eV with the dot size of 5 nm to 1.4 eV with 8 nm. As a conclusion, the Si species with PL at 1.9 eV should be the Si nanoparticles and they will be excluded from zeolite pores to grow in size.

The solvated Si species have three absorption maxima at 2.8, 3.1, and 3.5 eV in Figure 10. The species with absorption maxima at 2.8, 3.1, and 3.5 eV will be responsible for the PL species detected at 2.2 eV in Figure 3. *syn*-Tricyclooctane molecule with a ladder structure shows a luminescence peaked at 2.25 eV.[50] Layer-structured polysilanes show optical absorption spectra after annealing at different temperatures; that is, the band gap energy changes from about 2.5 to 1.1 eV.[51] PL in two-dimensional σ-conjugated organosilicon polymers such as polysilylenes and layered polysilanes has also been observed at 3.3 to 2.3 eV.[52,53] The Si quantum wires with 0.8 nm length and those with 5×5 Si atoms of 1.53 nm show nearly the same PL peaked at 2.1 eV.[54,55] These results imply that the PL photon energy can be influenced by the nature of nanosized Si species. The PL photon energy is almost similar and does not depend on the backbone length in the case of Si quantum wires. It will be reasonable to assign the PL component at 2.2 eV in our experiments to Si quantum wires. Here Si quantum wires mean the polysilanes terminated completely with hydrogen atoms. Then, the formed Si quantum wires should have different shapes and lengths because they will have absorption maxima at 2.8, 3.1, and 3.5 eV. As the temperature increases in hydrogen, the Si quantum wires in zeolite pores seem to change the Si nanoparticles, which will situate outside zeolite pores.

(b) PL Decay Characteristics of Si Species in Zeolite. So far visible PL spectra with relatively long lifetimes as much as some micro- to milliseconds have been observed in nanosized Si species. It is noted in the present study that the PL decay lifetimes of the Si species in zeolite pores are found to be independent of the PL photon energy and to be quite short, as much as 12 ns, even at 298 K in the PL component at 2.2 eV.

Two kinds of PL lifetimes have been detected in amorphous hydrogen-terminated nanosized Si species.[56,57] The PL components with longer (1 ms) and shorter (10 μs) lifetimes can be assigned to the possibility of a triplet and singlet excitonic state, respectively.[58] However, the PL component with the shorter decay lifetime can be observed discontinuously by terminating with C, N, and O atoms, and it is assumed that the distorted network structure cause the PL center to have a rather strongly localized structural configuration with a PL lifetime of about 1 ms.[31,56,58] The Si nanocrystals implanted into SiO_2 show PL spectra dependent both on the sizes and the passivation between Si and SiO_2 interfaces.[59] The PL decay lifetimes increase linearly with the diameter of the Si nanocrystals and exponentially with the wavelength in the microsecond region. It is explained by such that the radiative oscillator strength and the absorption cross-section become large in the smaller sized Si crystals. It has been accepted that the PL lifetime becomes shorter as the PL photon energy increases in Si nanoparticles both experimentally[33,35,60] and theoretically.[36] The PL of Si nanocrystals can be analyzed with the stretched-exponential function and shows nonexponential decays.[61] The factor in the function involves relations with the disorder and the energy transfer between nanocrystals.[62] In our experiments, PL decays obey the exponential form very nicely. As a result, our experimental results are different from these PL components; that is, the PL lifetimes are very short, as much as 12 ns, can be analyzed as simple first-order decay equations, and are almost constant with photon energies. Therefore, it is easily understood that the PL decay component at 2.2 eV in our experiments will not be the Si nanocrystals so far been reported.

The PL component at 2.14 eV is assigned to defects in SiO_2 in 1.5 nm amorphous Si in SiO_2, and the lifetime becomes short, as much as 3 ns, when temperature increases to 150 K.[32] It is

assumed that the PL lifetime is determined by the energy relaxation process in quantum wells and by the carrier diffusion into Si/SiO_2 interfaces. The nanosized Si species are prepared with pulsed laser deposition on SiO_2, and the observed PL at 2.1 eV have been similarly assigned to defects in SiO_2.[35,46] We consider that the PL of the defects in SiO_2 should be observed at 2.6 eV and the assignment of the PL component at 2.1 eV will also be reasonable since the Si/SiO_2 system involves the interface region with different conditions. The PL lifetime in hydrogen-terminated Si also decreases as the temperature for PL measurements increases.[59] On the other hand, the PL lifetime of the slower PL component at 1.4 eV is 1.5 ms at 5 K and becomes longer at room temperature to 160 ms in Si nanocrystals prepared with pulsed laser deposition in He.[35] They explain that the PL lifetimes become longer as temperature increases because of phonon dispersion. These results clearly suggest that the PL lifetime depends on the condition of nanospecies such as quantum-confined states and the interfaces with outer shells in the Si/SiO_2 system.

In our experiments the PL species can be observed around 2.2 eV, both in zeolite supercages and in HF solution, even at 298 K. The HF-solvated Si species should strongly be represented as the molecular state or the cluster state. They will be influenced significantly if they are confined in zeolite supercages. However, the difference between the PL photon energy of Si quantum wires in zeolite supercages and in HF solution is only 0.14 eV. Such a small energy difference can be explained by the energy dispersion through the zeolite lattice vibration at room temperature when Si quantum wires are encapsulated in zeolite supercages. In addition, it is noted that the PL intensities of Si quantum wires encapsulated in zeolite supercages are strong enough to be detected even at 298 K. It can be concluded that the Si quantum wires will be molecular states even in zeolite supercages and the PL photon energy can selectively be dissipated even at 298 K. Then, it will be probable that the PL lifetimes of the Si quantum wires could be quite short, as much as below 12 ns, which is close to the detection limit in our experimental setup.

References and Notes

(1) Meier, W. M.; Olson, D. H. *Atlas of Zeolite Structure Types*, Rev. Ed.; Butterworth-Heinemann: Oxford, U.K., 1992.

(2) Ozin, G. A.; Kuperman, A.; Stein, A. *Angew. Chem., Int. Ed. Engl.* **1989**, *28*, 359.

(3) Nozue, Y.; Kodaira, T.; Goto, T. *Phys. Rev. Lett*. **1992**, *68*, 3789.

(4) Nozue, Y. *J. Jpn. Phys. Soc. (Nihon Butsuri Gakkaishi)* **1993**, *48*, 624.

(5) Tamura, K.; Hosokawa, S.; Endo, H.; Yamasaki, S.; Oyanagi, H. *J. Phys. Soc. Jpn*. **1986**, *55*, 528.

(6) Parise, J. B.; MacDougall, J. E.; Herron, N.; Farlee, R.; Sleight, A. W.; Wang, Y.; Bein, T.; Moller, K.; Moroney, L. M. *Inorg. Chem*. **1988**, *27*, 221−228.

(7) Nozue, Y. *Solid Phys. (Kotai Butsuri)* **1991**, *26*, 367.

(8) Wang, Y.; Herron, N. *J. Phys. Chem*. **1988**, *92*, 4988.

(9) Stramel, R. D.; Nakamura, T.; Thomas, J. K. *J. Chem Soc., Faraday Trans. 1* **1988**, *84*, 1287.

(10) Herron, N.; Wang, Y.; Eddy, M. M.; Stucky, G. D.; Cox, D. E.; Moller, K.; Bein, T. *J. Am. Chem. Soc*. **1989**, *111*, 530.

(11) Fox, M. A.; Pettit, T. L. *Langmuir* **1989**, *5*, 1056.

(12) Stucky, G. D.; MacDougall, J. M. *Science* **1990**, *247*, 669.

(13) MacDougall, J. E.; Eckert, H.; Stucky, G. D. *J. Am. Chem. Soc*. **1989**, *111*, 8006.

(14) Cox, S. D.; Gier, T. E.; Stucky, G. D.; Bierlein, J. *J. Am. Chem. Soc*. **1988**, *110*, 2986.

(15) Wu, C.-G.; Bein, T. *Science* **1994**, *264*, 1757.

(16) Wu, C.-G.; Bein, T. *Science* **1994**, *266*, 1013.

(17) Launois, P.; Moret, R.; Bolloc'h, D. Le.; Albouy, P. A.; Tang, Z. K.; Li, G.; Chen, J. *Solid State Commun*. **2000**, *116*, 99.

(18) Werner, L.; Caro, J.; Finger, G.; Kornatoski, J. *Zeolites* **1992**, *12*, 658.

(19) Bein, T. In *Supramolecular Architecture*; Bein, T., Ed.; ACS Symposium Series 499; American Chemical Society: Washington, DC, 1992; Chapter 20.

(20) Choo, C.-K.; Sakamoto, T.; Tanaka, K.; Nakata, R.; Asakawa, T. *Appl. Surf. Sci*. **1999**, *140*, 126.

(21) Choo, C.-K.; Sakamoto, T.; Tanaka, K.; Nakata, R. *Appl. Surf. Sci*. **1999**, *148*, 116.

(22) Choo, C.-K.; Sakamoto, T.; Tohara, M.; Tanaka, K.; Nakata, R.; Okuyama, N. *Surf. Sci*. **2000**, *445*, 480.

(23) Choo, C.-K.; Enomoto, K.; Tanaka, K. *Mater. Sci. Eng. B* **2003**, *104*, 73.

(24) Ozin, G. A.; Dag, O.; Kuperman, A.; Macdonald, P. M. *Stud. Surf. Sci. Catal.* **1994**, *84*, 1107.

(25) Chomski, E.; Dag, G.; Kuperman, A.; Coombs, N.; Ozin, G. A. *Chem. Vap. Deposition* **1996**, *2*, 8.

(26) He, J.; Klug, D. D.; Tse, J. S.; Ratcliffe, C. I.; Preston, K. F. *Appl. Phys. Lett*. **1997**, *71*, 3194.

(27) He, J.; Ba, Y.; Ratcliffe, C. I.; Ripmeester, J. A.; Klug, D. D.; Tse, J. S. *Appl. Phys. Lett.* **1999**, *74*, 830.

(28) Canham, L. T. *Appl. Phys. Lett.* **1990**, *57*, 1046.

(29) Iyer, S. S.; Xie, Y.-H. *Science* **1993**, *260*, 40.

(30) Nihonyanagi, S.; Kanemitsu, Y. *Physica E* **2003**, *17*, 183.

(31) Oheda, H. *J. Non-Cryst. Solids* **2000**, *266*−*269*, 578.

(32) Kanemitsu, Y.; Iiboshi, M.; Kushida, T. *Appl. Phys. Lett.* **2000**, *76*, 2200.

(33) Kanamitsu, Y.; Fukunishi, Y.; Kushida, T. *Appl. Phys. Lett*. **2000**, *77*, 211.

(34) Kanamitsu, Y.; Fukunishi, Y. *Thin Solid Films* **2001**, *393*, 103.

(35) Watanabe, K.; Sawada, K.; Koshida, M.; Fujii, M.; Hayashi, S. *Appl. Surf. Sci*. **2002**, *197*−*198*, 635.

(36) Nishida, M. *Solid State Commun.* **2003**, *125*, 537.

(37) Tanaka, K.; Choo, C. K.; Komatsu, Y.; Hamaguchi, K.; Yamaki, M.; Itoh, T.; Nishigaya, T.; Nakata, R.; Morimoto, K. *J. Phys. Chem. B* **2004**, *108*, 2501.

(38) Tanaka, K.; Suzuki, S.; Choo, C. K. *J. Appl. Phys.* **2004**, *95*, 1287.

(39) Tanaka, K.; Suzuki, S.; Choo, C. K. *J. Appl. Phys.* **2004**, *95*, 1294.

(40) *Optical Processes in Semiconductors*; Pankove, J. I.; Dover: New York, 1971; Chapter 3.

(41) Tong, S.; Liu, X. N.; Gao, T.; Bao, X. M. *Appl. Phys. Lett.* **1997**, *71*, 698.

(42) Song, H. Z.; Bao, X. M.; Li, N. S.; Wu, X. L. *Appl. Phys. Lett.* **1998**, *72*, 356.

(43) Tohman, R.; Shimogaichi, Y.; Mizuno, H.; Ohki, Y.; Nagasawa, K.; Hama, Y. *Phys. Rev. Lett.* **1989**, *62*, 1388.

(44) Nishikawa, H.; Shiroyama, T.; Nakamura, R.; Ohki, Y.; Nagasawa, K.; Hama, Y. *Phys. Rev. B* **1992**, *45*, 586.

(45) Yamada, Y.; Orii, T.; Umezu, I.; Takeyama, S.; Yoshida, T. *Jpn. J. Appl. Phys.* **1996**, *35*, 1361.

(46) Makimura, T.; Kunii, Y.; Murakami, K. *Jpn. J. Appl. Phys.* **1996**, *35*, 4780.

(47) Li, S.; Silvers, S. J.; El-Sayed, M. S. *J. Phys. Chem. B* **1997**, *101*, 1794.

(48) Patrone, L.; Nelson, D.; Safarov, V. I.; Sentis, M.; Marine, W.; Giorgio, S. *J. Appl. Phys.* **2000**, *87*, 3829.

(49) Oda, S. *Mater. Sci. Eng. B* **2003**, *101*, 19.

(50) Kanemitsu, Y.; Suzuki, K.; Kyusin, S.; Matsumoto, H. *Phys. Rev. B* **1995**, *51*, 10666.

(51) Kawaji, H.; Yamanaka, S.; Shiotani, M. *Surf. Sci. (Hyomen Kagaku)* **1997**, *7*, 149.

(52) Wilson, W. L.; Weidman, T. W. *J. Phys. Chem*. **1991**, *95*, 4568.

(53) He, J.; Tse, J. S.; Klug, D. D.; Preston, K. F. *J. Mater. Chem*. **1998**, *8*, 705.

(54) Tyer, S. S.; Xie, Y. H. *Science* **1993**, *260*, 40.

(55) Shiraishi, K.; Ogawa, T.; Ohno, T.; Takeda, K.; Kanemitsu, Y. *Ohyo Butsuri (Appl. Phys.)* **1994**, *63*, 994.

(56) Oheda, H. *Phys. Rev. B* **1995**, *52*, 16530.

(57) Oheda, H. *J. Non-Cryst. Solids* **1996**, *198*−*200*, 284.

(58) Morigaki, K.; Yoshida, M. *J. Non-Cryst. Solids* **1987**, *90*, 139.

(59) Garcia, C.; Garrido, B.; Pellegrino, P.; Ferre, R.; Moreno, J. A.; Paveswi, L.; Cazzanelli, M.; Morante, J. R. *Physica E* **2003**, *16*, 429.

(60) Ookubo, N.; Hamada, N. *Solid State Commun.* **1994**, *92*, 369.

(61) Pavesi, L.; Cheschini, M. *Phys. Rev. B* **1993**, *48*, 17625.

(62) Priolo, F.; Franzo, G.; Pacifici, D.; Vincinguerra, V. *J. Appl. Phys.* **2001**, *89*, 264.